International Journal of Heat and Mass Transfer 135 (2019) 413–424

Contents lists available at ScienceDirect

International Journal of Heat and Mass Transfer

journal homepage: www.elsevier.com/locate/ijhmt

A numerical study on the thermal conductivity of $H_2O/CO_2/H_2$ mixtures in supercritical regions of water for coal supercritical water gasification system

Xueming Yang [a,*], Congcong Duan [a], Jiangxin Xu [a], Yuanbin Liu [b], Bingyang Cao [b,**]

[a] Department of Power Engineering, North China Electric Power University, Baoding 071003, China
[b] Key Laboratory for Thermal Science and Power Engineering of Ministry of Education, Department of Engineering Mechanics, Tsinghua University, Beijing 100084, China

ARTICLE INFO

Article history:
Received 27 August 2018
Received in revised form 23 January 2019
Accepted 31 January 2019

Keywords:
Thermal conductivity
Coal supercritical water gasification
Green-Kubo method
Equilibrium molecular dynamics simulation

ABSTRACT

Coal gasification technology is an important means of clean coal utilization. In the process of coal supercritical water gasification, $H_2O/CO_2/H_2$ or H_2O/CO_2 mixtures can be produced and used as the working medium for thermodynamic cycle power generation systems. The thermal conductivity of $H_2O/CO_2/H_2$ or H_2O/CO_2 mixtures is one of the most fundamental thermal properties required for the design and optimization of a thermodynamic system based on coal supercritical water gasification. Thus far, the thermal conductivity of $H_2O/CO_2/H_2$, H_2O/CO_2, and H_2O/H_2 mixtures in supercritical regions of water remains unknown. In this paper, the thermal conductivity of these mixtures in supercritical regions of water is predicted by equilibrium molecular dynamics (EMD) simulation and various theoretical models. The force field models and simulation strategies for the MD model are discussed and recommended. To validate the simulation method, the thermal conductivity of pure H_2O, CO_2, H_2 and CO_2/H_2 mixtures is calculated by MD simulations and compared with available experimental and NIST data. The method and data provided in this article may facilitate the practical applications of coal supercritical water gasification.

1. Introduction

Coal gasification technology plays an important role in current clean coal utilization technologies [1,2]. In recent years, supercritical water coal gasification and the related thermodynamic cycle power generation system have garnered extensive attention [3–5]. Guo et al. [4] proposed a novel thermal power generation system based on supercritical water gasification. In this system, coal and water are pumped into gasifier, and the organic matter of coal is completely gasified under supercritical water conditions and mainly converted into H_2, CO_2,(Coal $+ H_2O \rightarrow CO_2 + H_2$) and some precipitates of inorganic matter. The mixtures of supercritical water and clean H_2 and CO_2 flow out of reactor (gasifier) into the steam turbine to generate electricity. The power generation system based on coal supercritical water gasification offers many advantages, such as high coal-electricity efficiency, zero net CO_2 emissions, and no pollutants, thus showing good prospects [4,5].

The design and implementation of equipments for thermodynamic cycle power generation systems based on coal supercritical water gasification remains quite challenging. For example, the heat exchanger is a core component of the coal supercritical water gasification system and the thermodynamic cycle power generation system. The thermal conductivity of $H_2O/CO_2/H_2$ mixtures and H_2O/CO_2 mixtures are required in the design and optimization of heat exchangers. However, no reports and data are available for the thermal conductivity of $H_2O/CO_2/H_2$ mixtures and H_2O/CO_2 mixtures in supercritical regions of water. Although the thermodynamic and thermal transport properties of $H_2O/CO_2/H_2$ or H_2O/CO_2 mixtures can be evaluated from pure component data using theoretical calculation models, their reliability in near-critical and supercritical regions of water are questionable [6,7]. Therefore, a study on the thermodynamic properties of $H_2O/CO_2/H_2$ or H_2O/CO_2 mixtures in supercritical regions of water is of great significance for the development of coal supercritical water gasification and the design of thermodynamic cycle power generation system equipment. However, so far the thermal conductivity of H_2O/H_2 mixture, H_2O/CO_2 mixture and $H_2O/CO_2/H_2$ mixture in supercritical regions of water has not been studied.

* Corresponding author.
** Corresponding author.
E-mail addresses: xuemingyang@ncepu.edu.cn (X. Yang), caoby@tsinghua.edu.cn (B. Cao).

https://doi.org/10.1016/j.ijheatmasstransfer.2019.01.146
0017-9310/

Nomenclature

k_B	Boltzmann constant, 1.3806×10^{-23} J/K
P	system pressure, MPa
V	system volume, Å^3
T	system temperature, K
J	heat current vector, W/m^2
t	time, s
v_i	velocity of atom i, m/s
m_i	mass of atom i, kg
$\phi\ (r_{ij})$	potential energy between atoms i and j, J
r_{ij}	distance between atom i and atom j, Å
F_{ij}	force acting on atom i due to interactions with atom j, N
u_{ij}	interaction potential energy between molecules i and j, J
q	atomic charge, e
x	mole fraction
a	constant in Eq. (5)
b	constant in Eq. (5)
c	constant in Eq. (10)
M	molecular weight, g/mol
S	Sutherland constant, K
T_B	the boiling point at 1 atmosphere pressure, K

Greek symbols

λ	thermal conductivity, W·m^{-1}·K^{-1}
ε_{ij}^{kl}	depth of the L-J potential well between atoms i and j, eV
σ_{ij}^{kl}	characteristic distance in the L-J potential between atoms i and j, Å
ε_0	vacuum permittivity
η	viscosity, Pa·s
λ^0	translational thermal conductivity, W·m^{-1}·K^{-1}
ρ	density, kg/m^3

Subscript

i, j	refers to individual molecule i or j
k, l	refers to individual atom k or l
m	refers to mixture
Sim	simulation data
Exp	experimental data
NIST	Data from National Institute of Standards and Technology

Abbreviation

MD	Molecular Dynamics
EMD	Equilibrium Molecular Dynamics
RNEMD	Reverse Non-Equilibrium Molecular Dynamics
HCACF	Heat Current Autocorrelation Function
L-J	Lennard-Jones
KM	Keyes-Mass model
MS	Mason-Saxena model
LB	Lorentz-Berthelot
PPPM	Particle-Particle/Particle-Mesh
ARD	absolute relative deviation
AARD	averaged absolute relative deviation
ARE	absolute relative errors
AARE	averaged absolute relative errors

It is difficult to experimentally measure the thermal conductivity of pure or mixture fluids, especially at high temperature and high pressure, therefore, molecular dynamics (MD) simulations method becomes a good alternative. Aimoli et al. [8] used an equilibrium molecular dynamics (EMD) simulation to calculate the thermal conductivities of pure carbon dioxide in various force field models and compare it with experimental values, revealing an average simulation error of approximately 20%. Fernández et al. [9] performed EMD simulations to calculate the thermal conductivity of pure fluid (N_2, O_2, CO_2, C_2H_4), and their results agreed well with experimental results. Shvab et al. [10] calculated the thermal conductivity of pure water in the TIP4P/2005 model with EMD at a temperature of 670 K; the average error of the simulation compared with experimental values was approximately 30%. Song et al. [11] calculated the thermal conductivity of pure water using an SPC/E model with EMD simulations in the temperature range of 300–550 K. The average error when compared with experimental values was approximately 18%. Yu et al. [12] investigated the thermal conductivity of SiO_2/H_2O solid-gas system using EMD simulations with three different SiO_2/H_2O models. In addition, the NEMD methods, such as the perturbation method [13,14] and the direct method [15–20], are also effective alternatives for the calculation of thermal conductivity. By using the perturbation method, Matsunaga et al. [13] performed NEMD simulations on the thermal conductivity of the greenhouse gases carbon dioxide and methane dissolved in a sodium chloride aqueous solution. Römer et al. [15] investigated the thermal conductivity of pure water covering liquid and supercritical states using boundary driven molecular dynamics simulations. Bresme et al. [16] computed thermal conductivity of liquid water at high pressures and temperatures (1–50 kbar and 300–600 K) using RNEMD simulations. Mao et al. [17] computed the thermal conductivity of liquid water using reverse non-equilibrium molecular dynamics (RNEMD) from different force field models in a temperature range of 298–318 K. Trinh et al. [18] investigated the thermal conductivity of CO_2 with RNEMD in a temperature range of 300–1000 K and found the prediction errors for different models to increase in line with temperature. Although the RNEMD method has been used in studies of thermal conductivity for pure water or pure CO_2, it is still not applicable to the prediction of thermal conductivity of $H_2O/CO_2/H_2$ mixtures and H_2O/CO_2 mixtures due to the working principle of RNEMD.

Thus far, no report has evaluated the thermal conductivity of H_2O/H_2 binary mixtures, H_2O/CO_2 binary mixtures, or $H_2O/CO_2/H_2$ ternary mixtures in supercritical regions of water. In this paper, the thermal conductivity of these water–gas mixtures is predicted via EMD simulations. The adopted simulation method is validated, and the results are compared with those from the semi-empirical theoretical models. To facilitate comparison of the data in this work, all numerical data and uncertainty estimates are provided in the Data in Brief.

2. Methodology

2.1. Green-Kubo method

MD simulation is a popular methodology in investigating thermal conductivity of fluids and materials [19–23]. In EMD simulations, thermal conductivities of the fluids are calculated using the Green–Kubo formula, which establishes the relationship between the thermal conductivity and the time integral of the heat current autocorrelation function (HCACF). The average of the heat flux over the three coordinate directions generally enhances the statistical quality of results, and thus the ensemble average of the heat

current and its autocorrelation function can be used to estimate the thermal conductivity by

$$\lambda = \frac{1}{3k_B VT^2}\int_0^\infty \left\langle \vec{J}(0)\cdot\vec{J}(t)\right\rangle dt \tag{1}$$

where k_B is the Boltzmann constant, T is the system temperature, V is the volume of simulation domain, and $\vec{J}$ is the heat current at time t; $\left\langle \vec{J}(0)\cdot\vec{J}(t)\right\rangle$ is heat current autocorrelation function (HCACF).

The heat current is given by

$$\vec{J}(t) = \sum_i \vec{v}_i\vec{\varepsilon}_i + \frac{1}{2}\sum_{i,j,i\neq j}\vec{r}_{ij}\left(\vec{F}_{ij}\cdot\vec{v}_{ij}\right) \tag{2}$$

where $\vec{\varepsilon}_i$ is the atom total energy which means the sum of potential energy and kinetic energy, and is given by $\vec{\varepsilon}_i = \frac{1}{2}m_i\vec{v}_i^2 + \frac{1}{2}\sum_{j\neq i}\varphi(\vec{r}_{ij})$; $\phi(\vec{r}_{ij})$ is the inter-atomic potential energy between two neighboring atoms i and j, $\vec{v}_i$ is the velocity of particle i, $\vec{r}_{ij}$ is the distance between different position of atoms (σ), and $\varepsilon/k_B(K)$ is the force exerted by atom j on atom i.

2.2. Potentials for MD simulations

The potentials and the force fields play an important role in the process of molecular dynamics simulation. Therefore, it is important to choose appropriate potentials and force field models for the MD simulations in prediction of the thermal conductivity. In this study, the interaction between a pair of molecules, *i* and *j*, is calculated using the combined Lennard-Jones (LJ) and Coulomb potential as follows:

$$u_{ij} = \sum_{k=1}^{m}\sum_{l=1}^{n}\left\{4\varepsilon_{ij}^{kl}\left[\left(\frac{\sigma_{ij}^{kl}}{r_{ij}^{kl}}\right)^{12} - \left(\frac{\sigma_{ij}^{kl}}{r_{ij}^{kl}}\right)^{6}\right] + \frac{q_i^k q_j^l}{4\pi\varepsilon_0 r_{ij}^{kl}}\right\} \tag{3}$$

where u_{ij} is the interaction potential energy between molecules *i* and *j*, ε_{ij}^{kl} and σ_{ij}^{kl} are the interaction parameters of L-J potential which represent the energy parameter and scale parameter, respectively. r_{ij}^{kl} is the distance between atom *k* and atom *l*, q_i^k and q_j^l are the quantity of electric charge of *k* and *l*, respectively. ε_0 is the vacuum permittivity. The long-range electrostatic interactions are computed with the particle–particle particle-mesh (PPPM) method [24] with a cutoff distance of 12 Å and an accuracy of 10^{-4} in force. A cutoff distance of 12 Å is used for LJ interactions.

In this work, three commonly used models SPC/E [25], TIP4P [26], TIP4P/2005 [27] are adopted and compared in the prediction of the thermal conductivity for pure water. To describe the interaction of CO_2 molecules, the EPM2, EPM, and MSM3 rigid models, Cygan and TraPPE-flex flexible models are used and compared in the calculations of thermal conductivity of CO_2. Unlike the H_2O and CO_2 molecules, the types of the force field model for H_2 is less due to its simple structure, and there are two commonly used force field models for H_2, the two-site model [28] and single site model [29]. These two force field models for H_2 are comparable to each other and generally in good agreement with the experimental data because of the simple structure. The two-site model is used in this paper. Table 1 shows the force field parameters of the models used in this work. To describe the interactions between unlike atoms in the systems, the interaction parameters of the potential are obtained via the Lorentz-Berthelot mixing rule [30] which is the most commonly used combining rule [31].

Table 1
Force field parameters of the models used in this work.

Molecule	Model	Site	q (e)	σ (Å)	dOM (Å)	ε/k_B(K)
H_2O	SPC/E	O	−0.8476	3.166	–	78.197
		H	0.4238	–	–	–
	TIP4P	O	0	3.1536	–	78.02
		H	0.52	–	–	–
		M	−1.04	–	0.15	–
	TIP4P/2005	O	0	3.1589	–	93.2
		H	0.5564	–	–	–
		M	−1.1128	–	0.1546	–
CO_2	EPM2	C	0.6512	2.757	–	28.129
		O	−0.3256	3.033	–	80.507
	EPM	C	0.6645	2.785	–	28.99
		O	−0.33225	3.064	–	82.997
	MSM3	C	0.594	2.785	–	28.957
		O	−0.297	3.014	–	82.976
	Cygan	C	0.6512	2.8	–	28.144
		O	−0.3256	3.028	–	80.378
	TraPPE-flex	C	0.7	2.8	–	27.06
		O	−0.35	3.05	–	79.18
H_2	Two-site	H	–	2.72	–	10

2.3. Theoretical modes for the calculations of thermal conductivity of the mixtures

Although many theoretical models were proposed for the prediction of thermal conductivity of the mixtures, very few of them can be used for the ternary mixtures of $H_2O/CO_2/H_2$ due to the lack of the experimental values for the related binary interaction parameters in supercritical regions of water. Supercritical water has been considered to be nonpolar or weakly-polar. In this work, four theoretical models are adopted to compare with MD simulation results as follows: (1) KM model [32] for nonpolar gas mixtures; (2) KM model [33] for polar gas mixtures; (3) MS model [32] for nonpolar gas mixtures; (4) MS model [33] for polar gas mixtures.

The equations of the KM model to calculate the thermal conductivity of mixtures are as follows:

$$\lambda_m = \sum_{i=1}^{n}\frac{\lambda_i}{1+\frac{1}{x_i}\sum_{\substack{j=1\\ j\neq i}}^{n}A_{ij}x_j} \tag{4}$$

$$A_{ij} = \frac{1}{4}\left\{1+\left[\frac{\eta_i}{\eta_j}\left(\frac{M_j}{M_i}\right)^{a}\frac{\left(1+\frac{S_i}{T}\right)}{\left(1+\frac{S_j}{T}\right)}\right]^{1/2}\right\}^{2}\left(\frac{M_i+M_j}{2M_j}\right)^{b}\frac{\left(1+\frac{S_{ij}}{T}\right)}{\left(1+\frac{S_i}{T}\right)} \tag{5}$$

$$S = 1.5T_B \tag{6}$$

$$S_{12} = \sqrt{S_1S_2} \quad \text{for nonpolar gas mixtures} \tag{7}$$

$$S_{12} = 0.733\sqrt{S_1S_2} \quad \text{for polar gas mixtures} \tag{8}$$

where λ_m, λ_i are thermal conductivity of mixture and pure component, x_i, M_i, η_i are mole fraction, molecular weight and viscosity of component, respectively; T is temperature of mixtures, T_B is the boiling point of the pure component at 1 atmosphere pressure, and $T_{B,H2O}$ = 373 K, $T_{B,CO2}$ = 195 K. S are Sutherland constant, S_{H2} = 79 K [34]. The constants a and b are 0.75 and 0 respectively in KM model.

The equations of the MS model to calculate the thermal conductivity of mixtures are as follows:

$$\lambda_m = \sum_{i=1}^{n} \lambda_i \left(1 + \sum_{\substack{j=1 \\ j \neq i}}^{n} G_{ij} \frac{x_j}{x_i} \right)^{-1} \tag{9}$$

$$G_{ij} = \frac{c}{2\sqrt{2}} \left(1 + \frac{M_i}{M_j} \right)^{-\frac{1}{2}} \left[1 + \left(\frac{\lambda_i^0}{\lambda_j^0} \right)^{\frac{1}{2}} \left(\frac{M_i}{M_j} \right)^{\frac{1}{4}} \right]^2 \tag{10}$$

$$\frac{\lambda_i^0}{\lambda_j^0} = \frac{\eta_i M_j}{\eta_j M_i} \tag{11}$$

where λ_i is pure-component thermal conductivity, and x_i, x_j are mole fractions, M_i, M_j is molecular weight. λ^0 is the translational thermal conductivity, and η is viscosity. The constants c is set as 1.065 for nonpolar gas mixtures, and 0.85 for polar gas mixtures.

2.4. Molecular simulation details

The EMD simulations are performed for three-dimensional cubic box, and the periodic boundary conditions are applied in all X, Y and Z directions. All the MD simulations are carried out with the open source molecular dynamics simulator LAMMPS [35]. The time step is set as 1 fs for the pure fluid, and 0.4 fs for the mixtures. In all the simulations, the simulations initially run for 500,000 steps in NPT ensemble. Then switch to the NVT ensemble and equilibrate the system at a given temperature for 500,000 steps. The Nosé-Hoover thermostat is used in the NPT and NVT ensemble. Finally, it is switched to the NVE ensemble, the first 500,000 steps are performed to relax the system, and next 1,000,000 steps are used to calculate the heat current and thermal conductivity.

More details for the simulations can be found in the next section, including the adopted potentials, and the simulation strategy adopted and the details of process of the EMD simulation for the pure fluids and the mixtures.

3. Results and discussion

3.1. Predicting thermal conductivity using EMD simulation

The weak point of the Green–Kubo method for thermal conductivity calculation is that the uncertainties are much great in their each calculation. To obtain a correct description of thermal conductivity with EMD is to establish statistics from several results, starting from different initial conditions. More importantly, appropriate correlation time and enough long simulation time should be used.

To choose appropriate correlation times which are required for convergence, simulations are conducted to analyze the autocorrelation function and correlation time related thermal conductivity for the rigid SPC/E model of water molecule and the flexible model Cygan model of carbon dioxide molecule, and their hybrid model for the $H_2O/CO_2/H_2$ ternary mixtures. In the simulations, the temperature of 655 K and pressure of 25.2 MPa is set for the rigid SPC/E water model, temperature of 754.3 K and pressure of 19 MPa for the flexible Cygan carbon dioxide models (These conditions are selected to compare with the experimental study in Refs. [36,37]), and temperature of 873 K and pressure of 25 MPa for the hybrid model for the $H_2O/CO_2/H_2$ ternary mixtures. The analysis of the autocorrelation function and thermal conductivity are shown in Fig. 1. We conduct five independent simulations on pure fluid and mixtures by changing initial velocity. In this work, this ensures a good balance of accuracy and efficiency for the simulations [38,39]. Finally, an average thermal conductivity for the given temperature and pressure was evaluated by averaging over the values for the five independent runs, and the error estimate is obtained by the standard error of the values for each independent run.

The normalized HCACF for the rigid SPC/E water model is shown in Fig. 1(a). It can be observed that the HCACF decays fast to zero in 200 fs. However, for the flexible Cygan carbon dioxide models, it takes long correlation times (about 6000 fs) to sufficiently converge the HCACF, as shown in Fig. 1(c). These are consistent with the results by Sirk et al. [40] for the rigid and the flexible models for water. The correlation times (about 2500 fs) is needed to sufficiently converge the HCACF in the simulations of the $H_2O/CO_2/H_2$ ternary mixtures (as shown in Fig. 1(e)), where hybrid model is used by combining the rigid SPC/E water model, the flexible Cygan carbon dioxide model, and the two-site hydrogen model. Thus the correlation time needed for the hybrid model of $H_2O/CO_2/H_2$ ternary mixtures is between that for the rigid SPC/E water model and the flexible Cygan carbon dioxide model. In fact, the following two points should be considered when determine the duration of the correlation time windows τ: (1) The correlation time used to calculate the HCACF should be long enough to capture its full decay case; (2) longer correlation times will have larger statistical uncertainty because less data are available for its calculation. Therefore, in this work, we choose $\tau = 2$ ps for the simulations of pure fluids using rigid models, $\tau = 10$ ps for the simulations of pure fluids using flexible models, and $\tau = 4$ ps for the simulations of the mixtures.

The calculated thermal conductivities corresponding to the normalized HCACF for each model are also respectively shown in Fig. 1(b), (d) and (f), where the dashed line represents the results for each run, and the solid line represents the averaged thermal conductivity by five independent run. It can be observed that the methods and τ we adopted can ensure the convergence of the calculation of the thermal conductivity.

In each independent equilibrium run, the thermal conductivity calculated by numerical integration of the autocorrelation function will depend on the upper limit chosen for the time integral; we calculated an average value for each run by choosing 20 upper time limits spaced equally with 5τ. For example, the Fig. 2 shows the process of the calculation for each independent run and their average, which is corresponding to the results in Fig. 1(e) and (f). In Fig. 2(a), the solid line represents the averaged thermal conductivity by five independent run, and the dashed lines represents the results for each run which obtained from Fig. 2(b)–(f). The error estimate is obtained by the standard error of the average values for each independent run.

It should be noted that simulation strategies also significantly affect the accuracy. In Aimoli's simulation study [8], the thermal conductivity of CO_2 was calculated by an EMD production run of 2.5 ns which were divided into 5 equal intervals and the interval averages was used to estimate the predicted value. We find such a strategy may be less capable to deal appropriately with the uncertainties of EMD simulation. As described in our simulation strategies above, correct description of thermal conductivity with EMD is to establish statistics from several results, starting from different initial conditions. Here we calculated the thermal conductivity of at temperature of 328.15 K and density range of 200–800 kg/m^3 and compare with the simulation results by Aimoli et al. [8], as shown in Table 2. To clarify the ensuing discussion, the absolute relative errors (AREs) between the MD simulation results and those of the experiment (or data from NIST) [41] are calculated as $\mathrm{ARE} = \left|\lambda^{sim} - \lambda^{exp}\right| / \lambda^{\exp} \times 100\%$ or $\mathrm{ARE} = \left|\lambda^{sim} - \lambda^{NIST}\right| / \lambda^{NIST} \times 100\%$, where λ^{sim}, λ^{exp}, and λ^{NIST} denote the thermal conductivity values from MD simulations, experiments, and the NIST database, respectively. The average errors for the Cygan model and TraPPE-flex

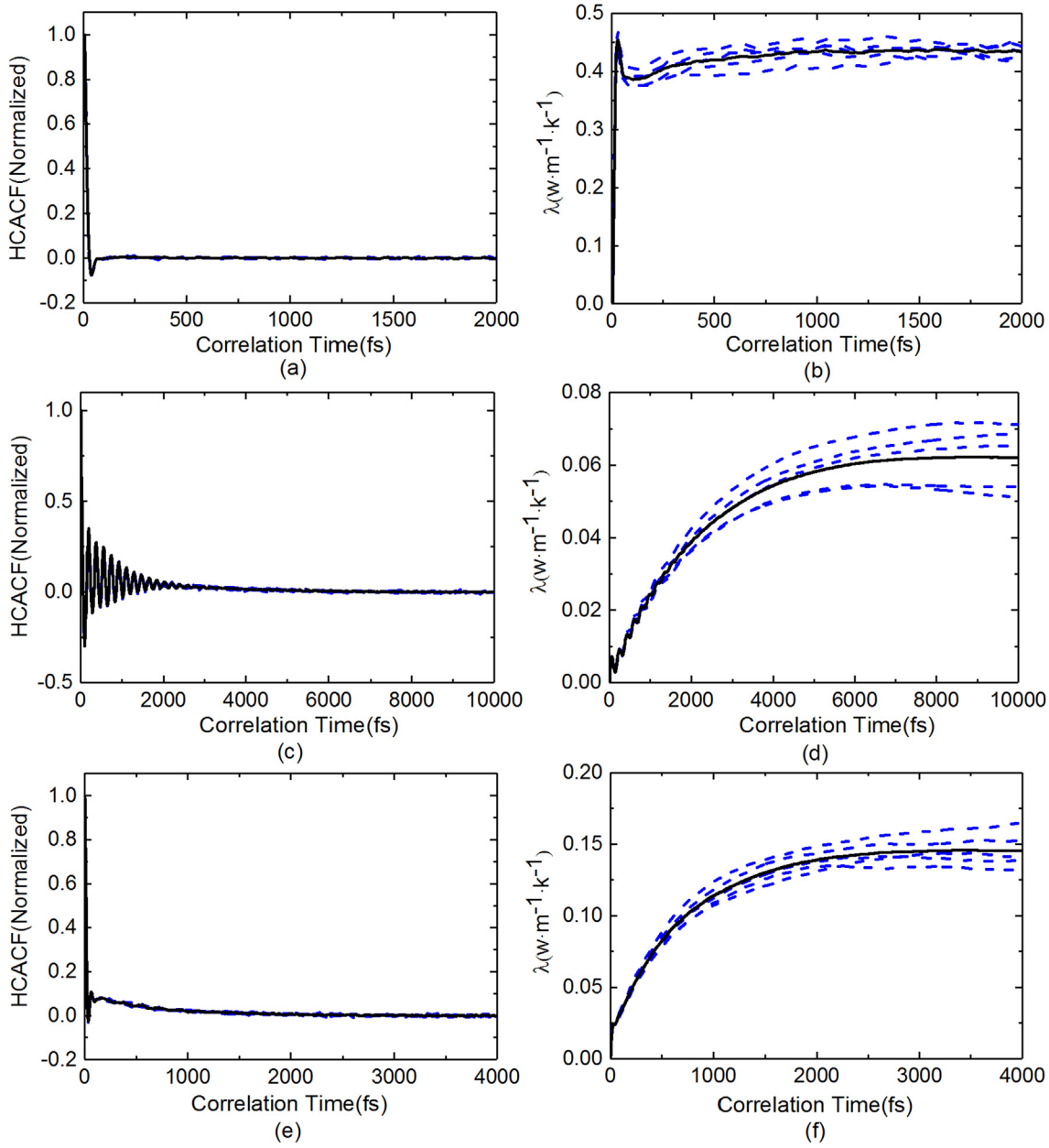

Fig. 1. The normalized HCACF and correlation time related thermal conductivity: (a), (b): rigid SPC/E water model (T = 655 K, P = 25.2 MPa); (c), (d): the flexible Cygan carbon dioxide model (T = 754.3 K, P = 19 MPa); (e), (f): hybrid model for $H_2O/CO_2/H_2$ ternary mixtures (T = 873 K, P = 25 MPa).

model by Aimoli et al are respectively 19.48% and 19.68%, however the average errors reduced to 8.76% and 9.19% by using our simulation strategies.

3.2. System size

Here we need to examine whether system size is playing a role in the simulation. A series of simulations with different system sizes, the total molecular number N = 1000, 2000, 3000, 4000, and 5000, are carried out and results are listed in Fig. 3. We find that the simulation results are consistent with each other within their uncertainties. It can be concluded that for the systems analyzed in this article, the calculated thermal conductivity using EMD is practically insensitive to system size. In fact, this is the main advantage of the EMD method thermal conductivity for thermal conductivity calculation compared to the NEMD methods.

3.3. Pure fluid

Given a lack of experimental data on the thermal conductivity of H_2O/H_2 binary mixtures, H_2O/CO_2 binary mixtures, and $H_2O/CO_2/H_2$ ternary mixtures, correct selection of force fields must be obtained by comparing experimental data and simulation results in pure fluids. First, the thermal conductivity of water is calculated via MD simulation at 655 K and pressures ranging from 24 MPa to 35 MPa. Three force field models of water are respectively adopted, and results are compared with experimental data in [36]. Results are shown in Fig. 4, revealing that the AREs of the SPC/E model are smallest with a value of 11.22%. The MD simulation results from the SPC/E model are also compared to experimental data from Leneindre et al. [37], as shown in Table 3. The average absolute relative error (AARE) is 10.28%, indicating that the simulation results of the SPC/E model agree relatively well with the experimental

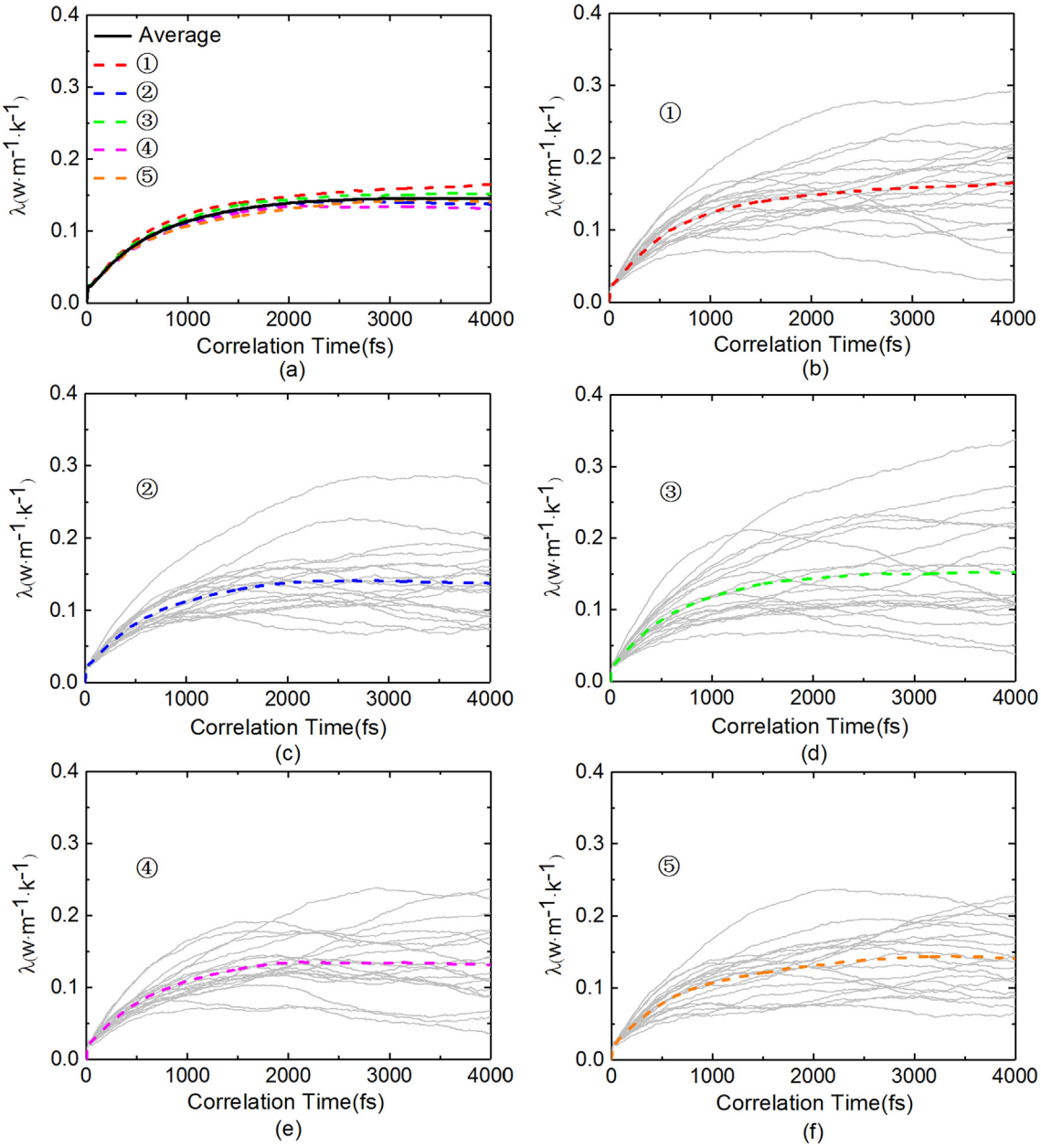

Fig. 2. Thermal conductivity calculated by numerical integration of the autocorrelation function in five independent run.

Table 2
Comparison of the thermal conductivity calculated by simulation strategies of Aimoli et al. [8] and this work.

ρ: kg/m^3	λ_{NIST}: W·m^{-1}·K^{-1}	Cygan (Aimoli)		TraPPE-flex (Aimoli)		Cygan (This work)		TraPPE-flex (This work)	
		λ: W·m^{-1}·K^{-1}	ARE	λ: W·m^{-1}·K^{-1}	ARE	λ: W·m^{-1}·K^{-1}	ARE	λ: W·m^{-1}·K^{-1}	ARE
200	0.0312	0.019	39.10%	0.019	39.10%	0.0304	2.56%	0.0294	5.77%
300	0.0424	0.028	33.96%	0.028	33.96%	0.0393	7.31%	0.041	3.30%
400	0.0533	0.041	23.08%	0.044	17.45%	0.0449	15.76%	0.046	13.70%
500	0.0606	0.055	9.24%	0.062	2.31%	0.0571	5.78%	0.0618	1.98%
600	0.0666	0.068	2.10%	0.074	11.11%	0.0746	12.01%	0.0709	6.46%
700	0.0756	0.081	7.14%	0.083	9.79%	0.0854	12.96%	0.0895	18.39%
800	0.0887	0.108	21.76%	0.110	24.01%	0.0931	4.96%	0.1018	14.77%
Average			19.48%		19.68%		8.76%		9.19%

data. Therefore, we recommend that the SPC/E model be used to predict the thermal conductivity of pure water.

For carbon dioxide, we choose five force field models for simulation at temperature of 450–850 K and pressure of 25 MPa; results are compared with NIST data. The error of the Cygan model is smallest (4.8%) as indicated in Fig. 5. We conduct additional simulations using the Cygan model and compare the results with experimental data [37]; see Table 4. The AARE is 10.27%.

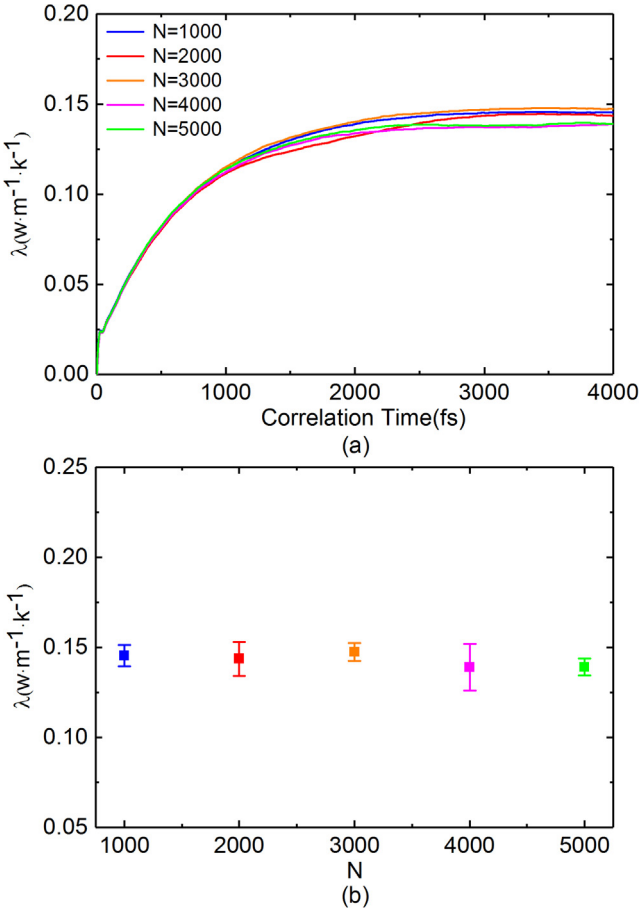

Fig. 3. The simulation results for $H_2O/CO_2/H_2$ mixtures with different system sizes.

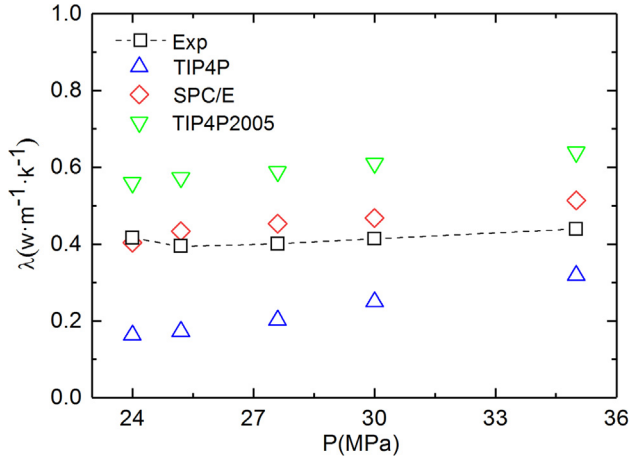

Fig. 4. Water force field comparison at temperature of 655 K.

Table 3
Comparison of simulation results and experimental values [37] for water molecule SPC/E model.

T: K	P: MPa	λ_{Exp}: W·m^{-1}·K^{-1}	λ_{Sim}: W·m^{-1}·K^{-1}	AREs (%)
712.4	20	0.0897	0.0946 ± 0.0012	5.46%
712.2	30	0.145	0.1733 ± 0.0035	19.5%
750.5	20	0.086	0.088 ± 0.0008	2.3%
749.9	30	0.117	0.1361 ± 0.0022	16.3%
784.6	20	0.0857	0.0797 ± 0.0016	7%
785.3	30	0.108	0.12 ± 0.0046	11.1%

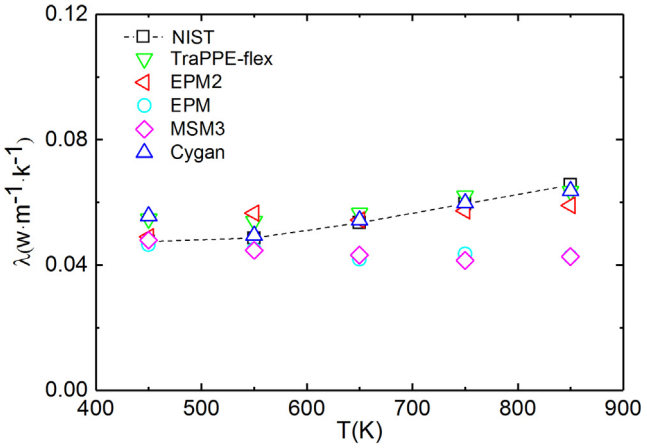

Fig. 5. Carbon dioxide force field comparison at pressure of 25 MPa.

Table 4
Comparison of simulation results and experimental values [37] for Carbon dioxide molecule Cygan model.

T: K	P: MPa	λ_{Exp}: W·m^{-1}·K^{-1}	λ_{Sim}: W·m^{-1}·K^{-1}	AREs (%)
645.4	19.3	0.0501	0.0538 ± 0.0017	7.39%
645.3	29.7	0.0541	0.0613 ± 0.0011	13.3%
680.9	20.6	0.0532	0.0596 ± 0.0021	12%
680.5	30.5	0.0568	0.0626 ± 0.0017	10.2%
754.3	19	0.0581	0.062 ± 0.0036	6.7%
753.6	29	0.0613	0.0687 ± 0.0025	12%

Table 5
Comparison of simulation results and experimental values [42] for hydrogen molecule two-site model.

T: K	P: MPa	λ_{Exp}: W·m^{-1}·K^{-1}	λ_{Sim}: W·m^{-1}·K^{-1}	AREs (%)
400	30	0.249	0.2473 ± 0.0054	0.68%
600	30	0.3198	0.3228 ± 0.0081	0.94%
800	30	0.3883	0.3592 ± 0.021	7.5%
1000	30	0.4577	0.4253 ± 0.0205	7.08%

For hydrogen gas, EMD simulations are carried out within a temperature range of 400–1000 K and a pressure of 30 MPa; results are listed and compared with experimental data [42] in Table 5. Results show that the AARE is 4.05%, indicating that the two-site model can accurately describe the thermal conductivity of hydrogen gas.

Through the above simulations, we recommend the SPC/E model for the water molecule, Cygan model for the carbon dioxide molecule, and two-site model for the hydrogen molecule when predicting the thermal conductivity of their mixtures.

3.4. CO_2/H_2 binary mixtures

Here we calculate the thermal conductivity via MD simulations for CO_2/H_2 mixtures (x_{CO_2}=50%, x_{H_2} = 50%) at a pressure of 25 MPa and temperature range 673–973 K. In fact, another purpose of this calculation is to evaluate the suitability of Lorentz-Berthelot mixing rule in supercritical regions of water in the lack of experimental data for H_2O/CO_2 mixture and $H_2O/CO_2/H_2$ mixtures. The results are compared with the data from NIST database [41] and the calculation results by the KM models and the MS models, as shown in Fig. 6. The AARE of the EMD model compared with NIST values is approximately 15.44%, while the AAREs of the theoretical models are 53.47–61.78%. Thus indicates that the results of the EMD

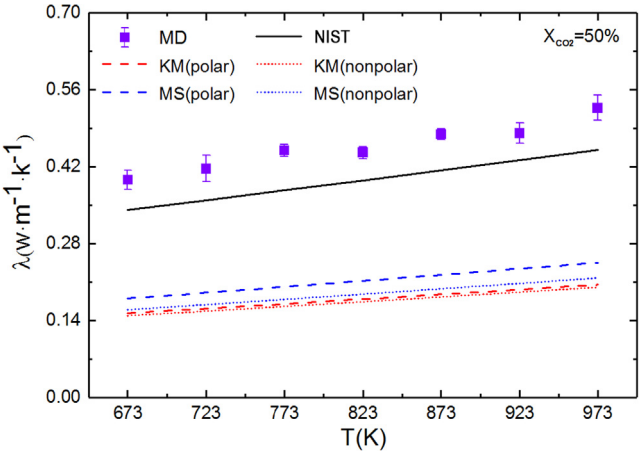

Fig. 6. Comparison of results calculated by EMD simulation and the theoretical models for CO_2/H_2 mixtures.

method are acceptable, while the predictions of KM and MS models are quite poor.

3.5. H_2O/CO_2 binary mixtures

Few experimental data are available under normal pressure and temperature to examine the thermal conductivity of H_2O/CO_2 mixtures [43,44]; however, the accuracy of these data needs to be verified. However, the accuracy of their data needs to be verified. For example, the experimental value of thermal conductivity in [43] is 0.02166 W m^{-1} K^{-1} at 0.1 MPa and 333 K for pure water (X_{H_2O}=100%, X_{CO_2} = 0), much less than the value of 0.6542 W m^{-1} K^{-1} per the NIST database [41]. Moreover, no experimental data and simulation results are available regarding the thermal conductivity of H_2O/CO_2 binary mixtures in supercritical regions. Here, we only compare our simulation results with those of semi-empirical theoretical models in a pressure range of 24–32 MPa and temperature of 850 K, as shown in Fig. 7.

To clarify the comparison, the absolute relative deviations (ARD) between the MD simulation results and calculation results using the theoretical models are calculated as follows:

$$\mathrm{ARD} = \left|\frac{\lambda^{sim} - \lambda^{calc}}{\lambda^{sim}}\right| \times 100\% \tag{12}$$

where λ^{sim} is the thermal conductivity calculated by MD simulations, and λ^{calc} is the value calculated with the semi-empirical theoretical models. When the CO_2 molar fractions (x_{CO_2}) in the mixtures are 5%, 10%, 15%, and 20%, respectively, the averaged ARDs (AARDs) between the MD simulation results and theoretical calculation results are 10.43–12.17%, 14.11–19.31%, 12.26–19.44%, and 9.24–16.02%, respectively. Fig. 7 shows that the thermal conductivities of H_2O/CO_2 mixtures increase along with rising pressure, and the ARDs decline roughly as the pressure increases.

3.6. H_2O/H_2 binary mixtures

Similarly, no data are available on the thermal conductivity of H_2O/H_2 binary mixtures in supercritical regions; thus, we only compare our simulation results with those from theoretical models in a pressure range of 24–32 MPa and temperature of 850 K, as displayed in Fig. 8. The ARDs increase with an increasing proportion of hydrogen. When the H_2 molar fractions (x_{H_2}) in the mixtures are

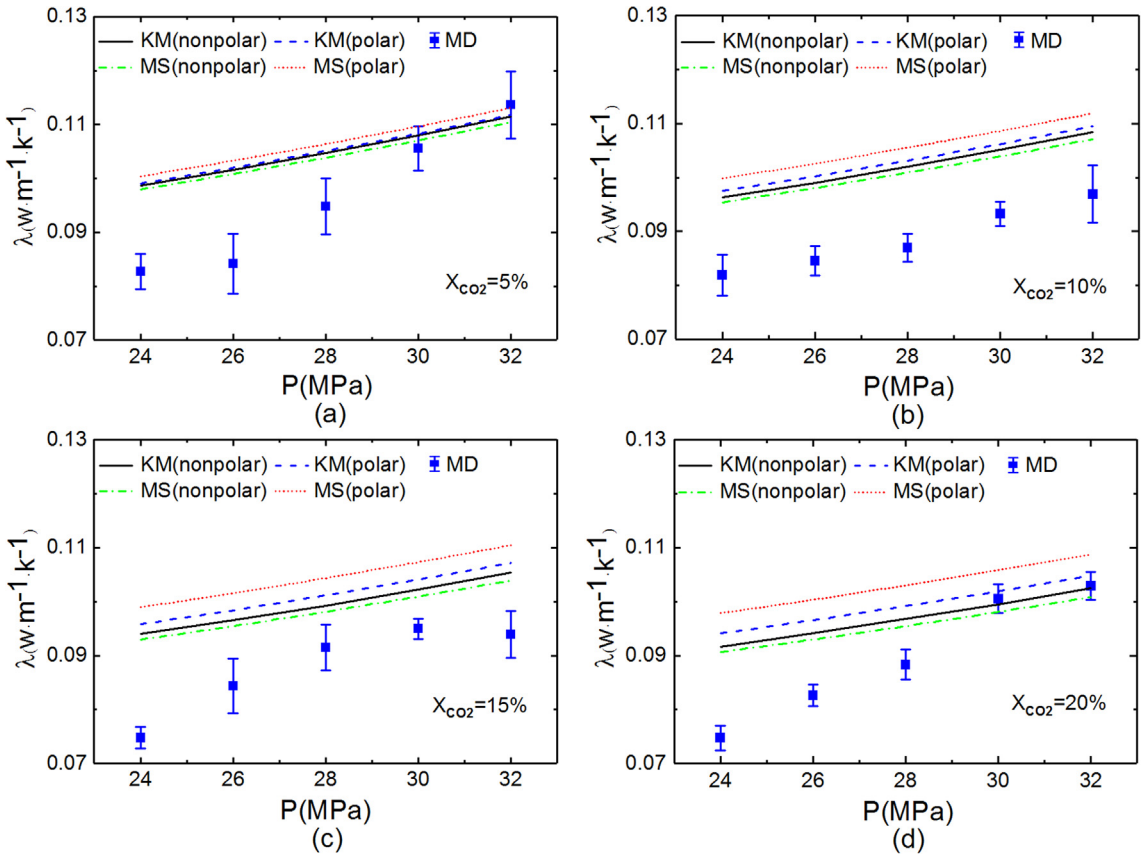

Fig.7. Predicted thermal conductivity of H_2O/CO_2 binary mixtures versus pressures at different x_{CO_2}.

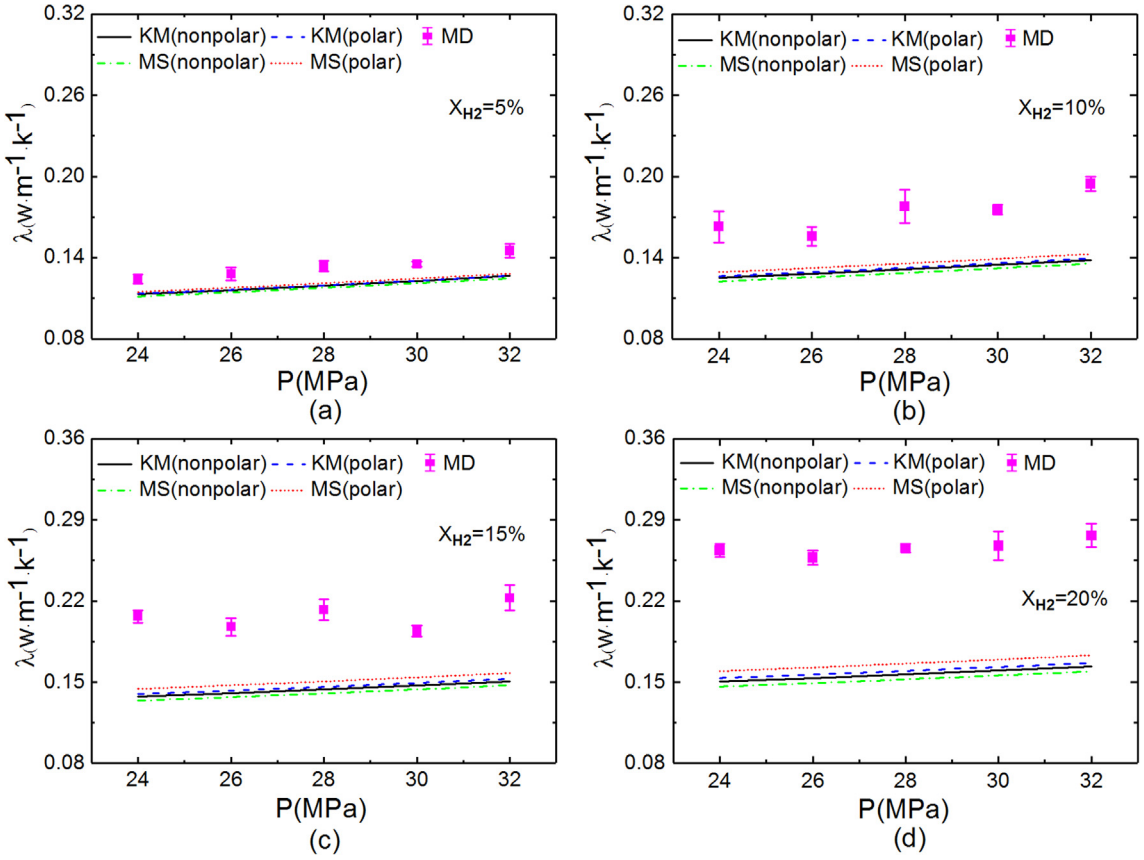

Fig. 8. Predicted thermal conductivity of H_2O/H_2 binary mixtures versus pressures at different x_{H_2} and their comparison with results from the theoretical modes.

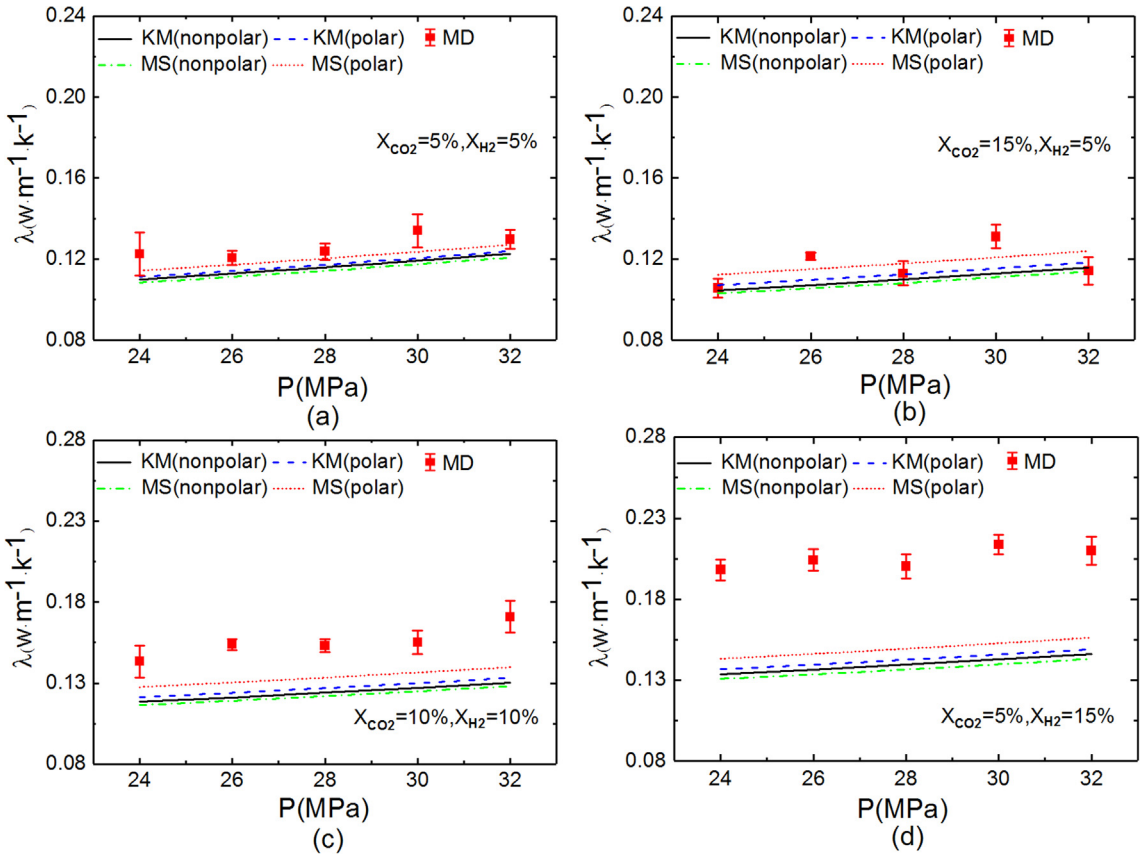

Fig. 9. Predicted thermal conductivity of $H_2O/CO_2/H_2$ ternary mixtures versus pressures at different x_{H_2} and x_{CO_2}.

5%, 10%, 15%, and 20%, respectively, the AARDs between the MD simulation results and theoretical calculation results are 8.86–11.52%, 21.35–25.41%, 26.88–31.88%, and 37.56–42.68%, respectively.

3.7. $H_2O/CO_2/H_2$ ternary mixtures

No studies have reported the thermal conductivity properties of $H_2O/CO_2/H_2$ ternary mixtures. As such, the calculated simulation results of $H_2O/CO_2/H_2$ ternary mixtures are compared with results from theoretical models in a pressure range of 24–32 MPa and a temperature of 850 K, as shown in Fig. 9. The data and corresponding ARDs in Fig. 9 are provided in Table S7 in the Data in Brief. The thermal conductivity of $H_2O/CO_2/H_2$ ternary mixtures increases roughly with increasing pressure. The AARDs between the MD simulation results and the theoretical calculation results are 4.44–9.22%, 5.45–7.04%, 13.87–21.26% and 27.04–33.29%, when x_{CO_2} and x_{H_2} are 5%, 5%; 15%, 5%; 10%, 10%; 5%, 15%, respectively. Therefore, the ARDs increase as the proportion of hydrogen increases.

Fig. 10 presents the results in a temperature range of 673–973 K and a pressure of 25 MPa. The data and corresponding ARD in Fig. 10 are provided in Table S8 of the Data in Brief. The AARDs between the MD simulation results and theoretical calculation results are 5.98–7.41%, 2.49–9.95%, 7.20–13.72% and 17.79–24.57%, when x_{CO_2} and x_{H_2} are 5%, 5%; 15%, 5%; 10%, 10%; 5%, 15%, respectively. In Fig. 10, as the temperature increases from 673 K to 973 K, the thermal conductivity of $H_2O/CO_2/H_2$ ternary mixtures declines first and then increases with increasing temperature. Such a temperature dependence of thermal conductivities in the given temperature range and pressure can be explained as follows: (1) thermal conductivity and viscosity of the water molecule decrease first and then increase with increasing temperature; (2) thermal conductivity of the pure CO_2 and H_2 increase steadily with increasing temperature; (thermal conductivity of the pure CO_2, pure H_2 and pure water are obtained from the NIST database [41] and the study conducted by Saini et al. [45]) (3) In Fig. 10, the water has the largest mole fraction in the mixtures. Based on the above reasons, the temperature dependence of thermal conductivities has characteristic minimum in Fig. 10.

3.8. Discussion

It should be noted that any evaluation for both the MD model and the semi-empirical theoretical models may be not possible in the lack of experimental data. The purpose of the study is only to compare their calculation results, and describe the discrepancy in these models and explain the possible reasons.

The above calculations reveal that the ARDs of thermal conductivities demonstrate a steady increase with increasing x_{H_2} for H_2O/H_2 binary mixtures and $H_2O/CO_2/H_2$ ternary mixtures in supercritical regions of water, and some of the ARDs of thermal conductivities reach more than 30% when $x_{H_2} \geqslant 15\%$. To investigate this discrepancy, further experimental data are needed on the thermal conductivity of H_2O/H_2 binary mixtures and $H_2O/CO_2/H_2$ ternary mixtures. With the aid of the experimental data in the future, the performance of both EMD models and the theoretical models could be improved in further.

As noted by Tan et al. [32], the predicted value by the KM model is influenced by the factors in Eq. (5): a, b, S_i, and S_{ij}. In the KM model, the values of a and b were obtained from experimental data on H_2/CO_2, H_2/N_2, H_2/Ar, and H_2/C_2H_4 at temperatures less than 353 K (80 °C). To generate a more accurate prediction, the factors

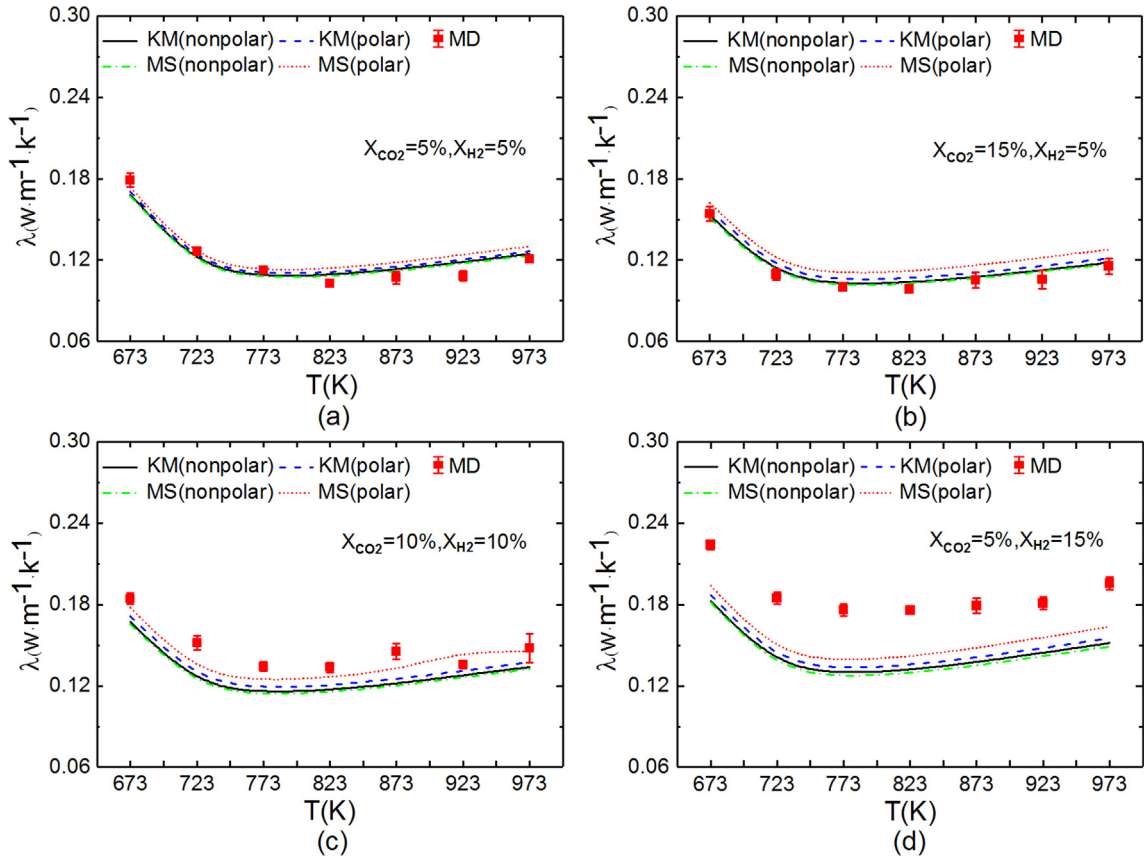

Fig. 10. Predicted thermal conductivity of $H_2O/CO_2/H_2$ ternary mixtures versus temperatures at different x_{H_2} and x_{CO_2}.

a and b should be obtained from experimental data for H_2O/H_2, H_2O/CO_2, and CO_2/H_2 binary mixtures at temperature and pressure in supercritical regions of water. In the KM model, it is not rigorous that the equations to calculate S_i were considered the same for all pure gases, and functions of S_{ij} were assumed to be the same for all gas mixtures [34]. In the MS model, the constant c in Eq. (10) is not well specified and was obtained from a study of measured thermal conductivities of binary rare gas mixtures. A better choice of the value for the constant c can enhance the performance of the MS model, especially when obtaining the value from experimental data for H_2O/H_2, H_2O/CO_2, and CO_2/H_2 binary mixtures at temperatures and pressures in supercritical regions of water.

Supercritical water has been considered nonpolar or weakly polar and is thought to possess a combination of gas and liquid properties along with the ability to dissolve nonpolar substances (e.g., hydrogen and other nonpolar gases). Different from the MD simulation in which the static and dynamic correlations, H-bonds and polarity for mixtures with water components have been considered, the semi-empirical theoretical models rely more on experimental data for pure components and their binary mixtures. In the absence of these experimental measurements, for theoretical calculation models, accurate prediction of the thermal conductivity of H_2O/H_2 binary mixtures, H_2O/CO_2 binary mixtures, and $H_2O/CO_2/H_2$ ternary mixtures in supercritical regions of water will likely remain challenging. On the other hand, to improve the prediction accuracy of the MD simulation method, better force field models should be highly recommended.

4. Conclusions

The thermal conductivity of $H_2O/CO_2/H_2$ mixtures is a prerequisite for the design and optimization of a heat exchanger system in a thermodynamic cycle power generation system based on coal supercritical water gasification. In this paper, the thermal conductivity properties of the H_2O/CO_2 binary mixtures, H_2O/H_2 binary mixtures, and $H_2O/CO_2/H_2$ mixtures in supercritical regions of water are investigated using EMD simulations. Simulation method for predicting thermal conductivity via EMD simulations is validated and recommended. To select appropriate force field models for prediction, the thermal conductivities of pure H_2O, CO_2, H_2 are calculated via EMD simulations with various force field models and compared with either available experimental data or data from NIST.

No data are available regarding the thermal conductivity of the H_2O/CO_2 binary mixture, H_2O/H_2 binary mixture, and $H_2O/CO_2/H_2$ mixtures in supercritical regions of water. In this work, prediction results of the thermal conductivity of these mixtures are compared with four different theoretical calculation models. For H_2O/CO_2 binary mixtures, the AARDs are found to be 9.24–19.44%. For H_2O/H_2 binary mixtures and $H_2O/CO_2/H_2$ ternary mixtures in supercritical regions of water, the AARDs of thermal conductivities show steadily increasing trend with increasing x_{H_2}. Some of the AARDs of thermal conductivities reach more than 30% when $x_{H_2} \geqslant 15\%$. Further experimental study of the thermal conductivity of H_2O/H_2 binary mixtures, H_2O/CO_2 binary mixtures, and $H_2O/CO_2/H_2$ ternary mixtures is strongly recommended to improve the prediction accuracy of EMD methods and theoretical calculation models. Resultant data in this work could offer useful information for the design and optimization of a thermodynamic system based on coal supercritical water gasification.

Conflicts of interest

The authors declare no competing financial interest.

Acknowledgments

This work was supported by the National Key R&D Program of China (Grant No. 2016YFB0600100).

Appendix A. Supplementary material

Supplementary data to this article can be found online at https://doi.org/10.1016/j.ijheatmasstransfer.2019.01.146.

References

[1] W. Chen, R. Xu, Clean coal technology development in China, Energy Pol. 38 (5) (2010) 2123–2130.
[2] Y. Gong, Q. Zhang, Q. Guo, Z. Xue, F. Wang, G. Yu, Vision-based investigation on the ash/slag particle deposition characteristics in an impinging entrained-flow gasifier, Appl. Energy 206 (2017) 1184–1193.
[3] J. Zhang, X. Weng, Y. Han, W. Li, J. Cheng, Z. Gan, J. Gu, The effect of supercritical water on coal pyrolysis and hydrogen production: a combined ReaxFF and DFT study, Fuel 108 (11) (2013) 682–690.
[4] L. Guo, H. Jin, Y. Lu, Supercritical water gasification research and development in China, J. Supercrit. Fluids 96 (2015) 144–150.
[5] L. Guo, H. Jin, Boiling coal in water: hydrogen production and power generation system with zero net CO2 emission based on coal and supercritical water gasification, Int. J. Hydrogen Energy 38 (29) (2013) 12953–12967.
[6] B. Todd, J.B. Young, Thermodynamic and transport properties of gases for use in solid oxide fuel cell modelling, J. Power Sources 110 (1) (2002) 186–200.
[7] X. Yang, J. Xu, S. Wu, M. Yu, B. Hu, B. Cao, J. Li, A molecular dynamics simulation study of PVT properties for H2O/H2/CO2 mixtures in near-critical and supercritical regions of water, Int. J. Hydrogen Energy 43 (24) (2018) 10980–10990.
[8] C.G. Aimoli, E.J. Maginn, C.R.A. Abreu, Transport properties of carbon dioxide and methane from molecular dynamics simulations, J. Chem. Phys. 141 (13) (2014) 134101.
[9] G.A. Fernández, J. Vrabec, H. Hasse, Shear viscosity and thermal conductivity of quadrupolar real fluids from molecular simulation, Mol. Simul. 31 (11) (2005) 787–793.
[10] I. Shvab, R.J. Sadus, Thermophysical properties of supercritical water and bond flexibility, Phys. Rev. E 92 (1) (2015) 012124.
[11] H.L. Song, Temperature dependence of the thermal conductivity of water: a molecular dynamics simulation study using the SPC/E model, Mol. Phys. 112 (16) (2014) 2155–2159.
[12] Y. Yu, Y. Tao, Y. He, Transport properties of SiO2/H2O solid-gas system for industrial flue gas: a molecular dynamics study, Int. J. Heat Mass Tran. 110 (2017) 723–729.
[13] S. Matsunaga, Effect of greenhouse gases dissolved in seawater, Int. J. Mol. Sci. 17 (1) (2016) 45.
[14] M. Yoshiya, A. Harada, M. Takeuchi, K. Matsunaga, H. Matsubara, Perturbed molecular dynamics for calculating thermal conductivity of zirconia, Mol. Simul. 30 (13–15) (2004) 953–961.
[15] F. Römer, A. Lervik, F. Bresme, Nonequilibrium molecular dynamics simulations of the thermal conductivity of water: a systematic investigation of the SPC/E and TIP4P/2005 models, J. Chem. Phys. 137 (7) (2012) 074503.
[16] F. Bresme, F. Römer, Heat transport in liquid water at extreme pressures: a non equilibrium molecular dynamics study, J. Mol. Liq. 185 (2013) 1–7.
[17] Y. Mao, Y. Zhang, Prediction of the temperature-dependent thermal conductivity and shear viscosity for rigid water models, J. Nanotechnol. Eng. Med. 3 (3) (2012) 2981–2984.
[18] T.T. Trinh, T.J.H. Vlugt, S. Kjelstrup, Thermal conductivity of carbon dioxide from non-equilibrium molecular dynamics: a systematic study of several common force fields, J. Chem. Phys. 141 (13) (2014) 134504.
[19] G.C. Pan, J. Ding, W. Wang, J. Lu, J. Li, X. Wei, Molecular simulations of the thermal and transport properties of alkali chloride salts for high-temperature thermal energy storage, Int. J. Heat Mass Transf. 103 (2016) 417–427.
[20] J. Gonzalez, J. Ortega, Z. Liang, Prediction of thermal conductance at liquid-gas interfaces using molecular dynamics simulations, Int. J. Heat Mass Transf. 126 (2018) 1183–1192.
[21] C. Jiang, J. Ouyang, L. Wang, Q. Liu, X. Wang, Transport properties and structure of dense methane fluid in the rough nano-channels using non-equilibrium multiscale molecular dynamics simulation, Int. J. Heat Mass Transf. 110 (2017) 80–93.
[22] S. Srinivasan, M.S. Diallo, S.K. Saha, O.A. Abass, A. Sharma, G. Balasubramanian, Effect of temperature and graphite particle fillers on thermal conductivity and viscosity of phase change material n-eicosane, Int. J. Heat Mass Transf. 114 (2017) 318–323.
[23] Hua Bao, Jie Chen, Xiaokun Gun, Bingyang Cao, A review of simulation methods in micro/nanoscale heat conduction, ES Energy Environ. 1 (2018) 16–55.
[24] R.W. Hockney (Ed.), Computer Simulation Using Particles, Taylor & Francis, New York, NY, USA, 1988.

[25] H.J.C. Berendsen, J.R. Grigera, T.P. Straatsma, The missing term in effective pair potentials, J. Phys. Chem. 91 (24) (1987) 6269–6271.
[26] W.L. Jorgensen, J. Chandrasekhar, J.D. Madura, R.W. Impey, M.L. Klein, Comparison of simple potential functions for simulating liquid water, J. Chem. Phys. 79 (2) (1983) 926–935.
[27] J.L.F. Abascal, C. Vega, A general purpose model for the condensed phases of water: TIP4P/2005, J. Chem. Phys. 123 (23) (2005) 234505.
[28] R.F. Cracknell, Molecular simulation of hydrogen adsorption in graphitic nanofibres, PCCP 3 (11) (2001) 2091–2097.
[29] V. Buch, Path integral simulations of mixed para-D2 and ortho-D2 clusters: the orientational effects, J. Chem. Phys. 100 (10) (1994) 7610–7629.
[30] M.P. Allen, D.J. Tildesley, Computer Simulation of Liquids, Oxford University Press, 1989.
[31] T. Akıner, H. Ertürk, K. Atalık, Prediction of thermal conductivity and shear viscosity of water-Cu nanofluids using equilibrium molecular dynamics, ASME 2013 International Mechanical Engineering Congress and Exposition, American Society of Mechanical Engineers, 2013.
[32] Y. Tan, W. Nookuea, H. Li, E. Thorin, J. Yan, Evaluation of viscosity and thermal conductivity models for CO2 mixtures applied in CO2 cryogenic process in carbon capture and storage (CCS), Appl. Therm. Eng. 123 (2017) 721–733.
[33] P.K. Tondon, S.C. Saxena, Calculation of thermal conductivity of polar-nonpolar gas mixtures, Appl. Sci. Res. 19 (1) (1968) 163–170.
[34] A.L. Lindsay, L.A. Bromley, Thermal conductivity of gas mixtures, Ind. Eng. Chem. 42 (8) (1950) 1508–1511.
[35] S. Plimpton, Fast parallel algorithms for short-range molecular dynamics, Academic Press Professional 117 (1–19) (1995).
[36] R. Tufeu, B.L. Neindre, Thermal conductivity of steam from 250 to 510°C at pressures up to 95 MPa including the critical region, Int. J. Thermophys. 8 (3) (1987) 283–292.
[37] B. Leneindre, R. Tufeu, P. Bury, J.V. Sengers, Thermal conductivity of carbon dioxide and steam in the supercritical region, Ber. Bunsenges. Phys. Chem. 77 (4) (1973) 262–275.
[38] R. Khare, J. de Pablo, A. Yethiraj, Molecular simulation and continuum mechanics study of simple fluids in non-isothermal planar couette flows, J. Chem. Phys. 107 (7) (1997) 2589–2596.
[39] A.J.H. McGaughey, M. Kaviany, Thermal conductivity decomposition and analysis using molecular dynamics simulations, Part I. Lennard-Jones argon, Int. J. Heat Mass Transf. 47 (8–9) (2004) 1783–1798.
[40] T.W. Sirk, S. Moore, E.F. Brown, Characteristics of thermal conductivity in classical water models, J. Chem. Phys. 138 (6) (2013) 064505.
[41] E.W. Lemmon, M.L. Huber, M.O. McLinden, NIST Standard Reference Database 23: Reference Fluid Thermodynamic and Transport Properties-REFPROP, Version 9.1, National Institute of Standards and Technology, Standard Reference Data Program, Gaithersburg, 2013.
[42] M.J. Assael, J.A.M. Assael, M.L. Huber, R.A. Perkins, Y. Takata, Correlation of the thermal conductivity of normal and parahydrogen from the triple point to 1000 K and up to 100 MPa, J. Phys. Chem. Ref. Data 40 (3) (2011) 033101.
[43] K.M. Dijkema, J.C. Stouthart, D.A.D. Vries, Measurements of the thermal conductivity of gases and gas mixtures, methods and results, Wärme – und Stoffübertragung 5 (1) (1972) 47–55.
[44] H. Li, Ø. Wilhelmsen, Y. Lv, W. Wang, J. Yan, Viscosities, thermal conductivities and diffusion coefficients of CO2 mixtures: review of experimental data and theoretical models, Int. J. Greenhouse Gas Control 5 (5) (2011) 1119–1139.
[45] V. Saini, A. Kumar, P.R. Usurumarti, R.S. Dondapati, Development of correlations for the specific heat and thermal conductivity of supercritical water used as coolant in nuclear power plant technology.